applied sciences

MDPI

Article

Evaluation of Grouting Effectiveness on Cracks in Cement-Stabilized Macadam Layer Based on Pavement Mechanical Response Using FBG Sensors

Min Zhang [1], Hongbin Hu [1], Cheng Ren [2], Zekun Shang [2] and Xianyong Ma [2,*]

[1] Guangzhou Suihua Intellignet Traffic Technology Co., Ltd., Guangzhou 510080, China; zm646049648@gmail.com (M.Z.); huhongbin84@gmail.com (H.H.)
[2] School of Transportation Science & Engineering, Harbin Institute of Technology, Harbin 150090, China; rencheng111@foxmail.com (C.R.); 15822252948@163.com (Z.S.)
* Correspondence: maxianyong@hit.edu.cn

Featured Application

This study provides a method for evaluating the effect of crack grouting in semi-rigid bases.

Abstract

Cracking in semi-rigid cement-stabilized macadam bases constitutes a prevalent distress in asphalt pavements. While extensive research exists on grouting materials for crack rehabilitation, quantitative assessment methodologies for treatment efficacy remain underdeveloped. This study proposes a novel evaluation framework integrating fiber Bragg grating (FBG) technology to monitor pavement mechanical responses under traffic loads. Conducted on the South China Expressway project, the methodology encompassed (1) a method for back-calculating the modulus of the asphalt layer based on Hooke's Law; (2) a sensor layout plan with FBG sensors buried at the top of the pavement base in seven sections; (3) statistical analysis of the asphalt modulus based on the mechanical response when a large number of vehicles passed; and (4) comparative analysis of modulus variations to establish quantitative performance metrics. The results demonstrate that high-strength geopolymer materials significantly enhanced the elastic modulus of the asphalt concrete layer, achieving 34% improvement without a waterproofing agent versus 19% with a waterproofing agent. Polymer-treated sections exhibited a mean elastic modulus of 676.15 MPa, substantially exceeding untreated pavement performance. Low-strength geopolymers showed marginal improvements. The modulus hierarchy was as follows: high-strength geopolymer (without waterproofing agent) > polymer > high-strength geopolymer (with waterproofing agent) > low-strength geopolymer (without waterproofing agent) > low-strength geopolymer (with waterproofing agent) > intact pavement > untreated pavement. These findings demonstrate that a high-strength geopolymer without a waterproofing agent and high-polymer materials constitute optimal grouting materials for this project. The developed methodology provides critical insights for grout material selection, construction process optimization, and post-treatment maintenance strategies, advancing quality control protocols in pavement rehabilitation engineering.

Keywords: semi-rigid base asphalt pavement; mechanical response; reflective cracks; evaluation of grouting treatment effect; FBG technology

check for updates

Academic Editors: Andrea Carpinteri and Eleni Tsangouri

Received: 3 April 2025
Revised: 15 May 2025
Accepted: 26 June 2025
Published: 28 June 2025

Citation: Zhang, M.; Hu, H.; Ren, C.; Shang, Z.; Ma, X. Evaluation of Grouting Effectiveness on Cracks in Cement-Stabilized Macadam Layer Based on Pavement Mechanical Response Using FBG Sensors. *Appl. Sci.* **2025**, *15*, 7312. https://doi.org/10.3390/app15137312

Copyright: © 2025 by the authors. Licensee MDPI, Basel, Switzerland. This article is an open access article distributed under the terms and conditions of the Creative Commons Attribution (CC BY) license (https://creativecommons.org/licenses/by/4.0/).

1. Introduction

Semi-rigid base asphalt pavements, characterized by their high load-bearing capacity and cost-effectiveness [1], represent one of China's predominant pavement structures. However, they are prone to cracking due to temperature fluctuations, moisture variations, and traffic loading [2,3]. The South China Expressway (SCE), notable for its ultra-wide cross-sections, heavy traffic volumes, and extended service periods, has faced structural challenges stemming from uneven subgrade compaction during initial construction. This deficiency has led to semi-rigid base cracking under heavy-duty traffic. Compounded by environmental factors such as high temperatures, abundant rainfall, and karst geology along the route, water infiltration through the subgrade accumulates within base layer cracks, ultimately inducing reflective cracking in the pavement surface. Traditional repair techniques, particularly those targeting substructures, often necessitate extensive pavement destruction, generating substantial waste materials and significant carbon emissions. As a minimally invasive rehabilitation method, grouting technology has gained prominence in base layer stabilization due to its rapid implementation, trenchless nature, and operational safety [4]. Nevertheless, systematic evaluation criteria for treatment efficacy and research on critical process parameters remain underdeveloped, limiting their optimization for complex engineering scenarios like the SCE.

Grouting technologies are primarily classified into five material-based categories: polymer, early-strength low-strength geopolymer, early-strength low-strength waterproof geopolymer, early-strength high-strength geopolymer, and early-strength high-strength waterproof geopolymer. Studies on polymer grouting materials reveal critical mechanical and durability properties. Fang et al. [5] demonstrated that increasing material density induces exponential growth in yield strength, elastic modulus, and secant modulus, accompanied by a logarithmic increase in Poisson's ratio. Wang et al. [6] investigated corrosion resistance, identifying minimal water-induced strength degradation but significant reductions in acidic/alkaline environments, with corrosion effects intensifying over time. Zhang et al. [7] investigated the effects of different components on response variables and determined the optimal formulation of polymer grouting material using a multi-objective optimization approach. In the research on geopolymer grouting materials, Peng et al. [8] compared geopolymer and Portland cement concrete, demonstrating the former's superior resistance to chemical erosion, chloride ion penetration, and freeze–thaw cycles. Sarıdemir et al. [9] found that geopolymer concrete exhibits superior corrosion resistance, with Portland cement concrete demonstrating approximately 51% greater strength loss than geopolymer concrete under identical corrosive conditions. Mukhtar et al. [10] further enhanced geopolymer performance through mechanochemical activation, which reduced slurry rheological complexity while improving unconfined compressive strength. While material properties dominate existing research, emerging studies focus on grouting rehabilitation effectiveness. Li et al. [11] numerically analyzed mechanical response variations in pavements before and after polymer grouting. Zhu et al. [12] established a comprehensive evaluation method integrating radar simulation and empirical measurements, utilizing time–frequency-domain signal characteristics to effectively assess grouting treatment effectiveness for semi-rigid pavement base layer cracks, validated through engineering case analysis and field coring verification. Zhang et al. [13] developed a fatigue damage model for semi-rigid base asphalt pavement structures and established a three-dimensional numerical model using the finite element method. They further conducted a comparative analysis of the mechanical responses and fatigue damage conditions of the pavement before and after polymer repair. Li et al. [14] derived critical grouting effectiveness criteria through shear testing and numerical simulations.

Existing studies have extensively investigated the mechanical and physicochemical properties of commonly used polymer and geopolymer grouting materials through experimental validation. However, current research on evaluating the effectiveness of asphalt pavement grouting primarily relies on deflection values measured by falling weight deflectometers (FWDs). This method is time-consuming, labor-intensive, and susceptible to testing conditions and fails to reflect the structural stress response under vehicular loads. Although some scholars have employed finite element analysis to study mechanical behaviors before and after grouting, the lack of field-measured data undermines the reliability of numerical simulations.

Fiber Bragg grating (FBG) sensing technology, one of the most rapidly advancing high-tech applications in civil engineering [15], has gained increasing attention in pavement engineering for temperature field monitoring [16,17] and strain field measurements [18,19]. Nevertheless, its application in holistic pavement rehabilitation assessment remains limited. Traditional evaluation methods focus on static performance improvements, neglecting dynamic stress–strain tracking and mechanical interactions between treated and adjacent areas. This study proposes a quantitative evaluation method for the grouting treatment of defects in semi-rigid base asphalt pavements, integrating FBG monitoring technology with structural mechanics analysis. The methodology provides critical guidance for the design of grouting reinforcement materials, the optimization of injection processes, and post-treatment structural maintenance strategies.

2. Principle and Mathematical Model

2.1. Principle of FBG Sensor

This study employed FBG sensors for data acquisition. The fundamental principle involves measuring the shift in the reflected central wavelength to quantify temperature and strain variations [20]. For an FBG sensor (Figure 1), the Bragg wavelength λ_B, defined as the central wavelength reflected when incident light interacts with the grating, is expressed as [21]

$$\lambda_B = 2n_{eff}\Lambda \tag{1}$$

where n_{eff} represents the effective refractive index of the fiber core, and Λ denotes the grating period.

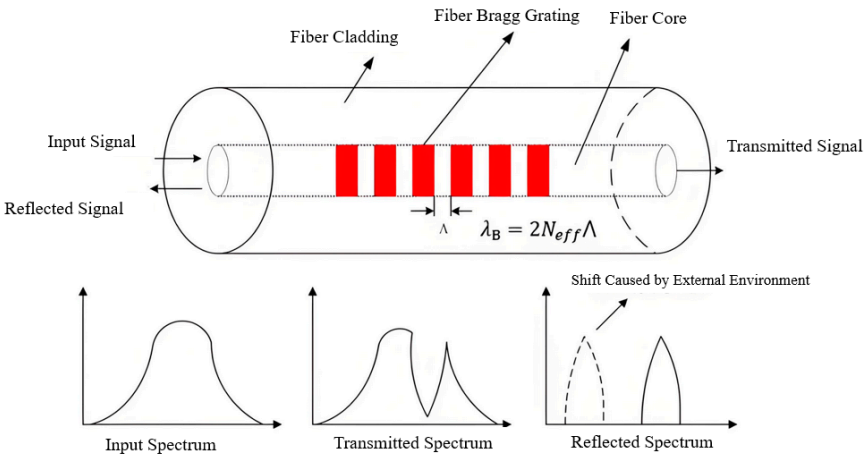


Figure 1. Schematic of FBG sensor.

The wavelength shift in an FBG induced by temperature (ΔT) and strain (ε) is mathematically represented as

$$\frac{\Delta\lambda_B}{\lambda_B} = (\alpha_s + \xi_s)\Delta T + (1 - P_\varepsilon)\varepsilon \tag{2}$$

where α_s is the thermal expansion coefficient of the optical fiber, ξ_s is the thermo-optic coefficient of the optical fiber, and P_ε is the effective photoelastic coefficient of the optical fiber.

A further simplified equation is

$$\frac{\Delta\lambda_B}{\lambda_B} = \alpha_T \Delta T + \alpha_\varepsilon \varepsilon \tag{3}$$

where $\alpha_T = \alpha_s + \xi_s$ is the temperature sensitivity coefficient, and $\alpha_\varepsilon = 1 - P_\varepsilon$ is the strain sensitivity coefficient.

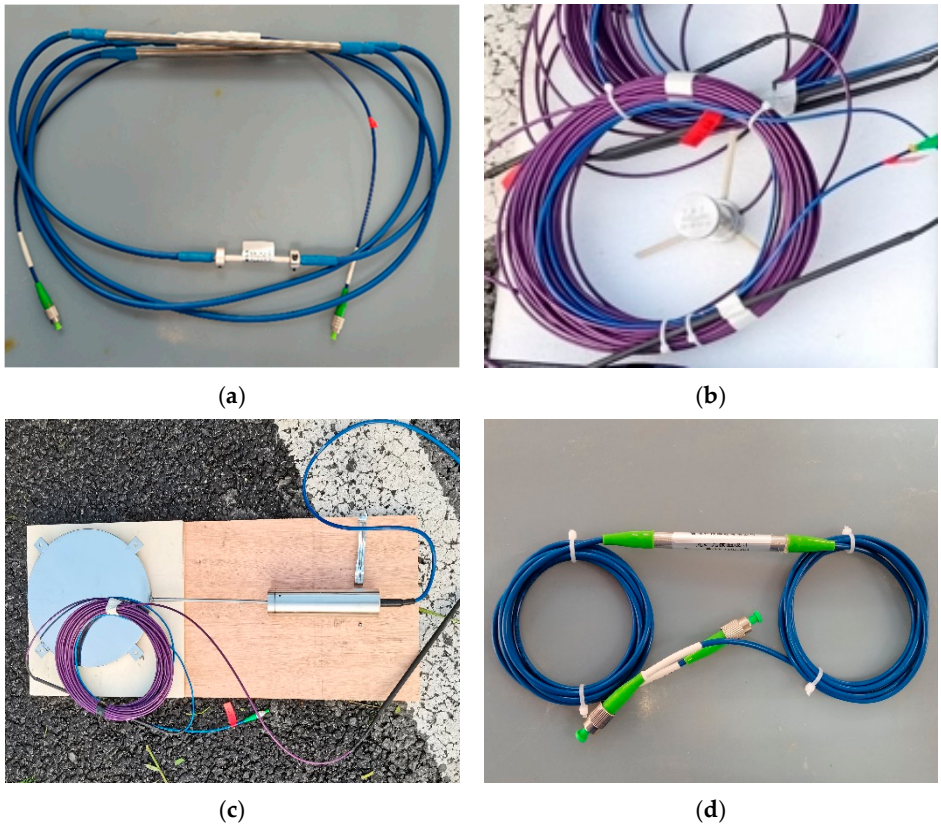
For FBG temperature sensors, under the assumption of negligible external mechanical loading, where wavelength shifts are exclusively caused by temperature variations, the governing relationship is expressed as

$$\Delta\lambda_B = \alpha_T \Delta T \lambda_B \tag{4}$$

This unique characteristic enables the fabrication of FBG temperature sensors, where temperature monitoring is achieved by detecting variations in the reflected wavelength.

For FBG strain sensors, calibration experiments determine the temperature sensitivity coefficient (α_T) and strain sensitivity coefficient (α_ε). By deploying auxiliary temperature sensors adjacent to the strain sensors to monitor thermal fluctuations, structural strain can be computationally derived through thermal compensation algorithms.

The FBG sensors utilized in this study are schematically illustrated in Figure 2.



(**a**) (**b**) (**c**) (**d**)

Figure 2. FBG sensors of this study. (**a**) Horizontal strain sensor; (**b**) vertical strain sensor; (**c**) Earth pressure sensor; (**d**) temperature sensor.

2.2. Modulus Back-Calculation Method

The current pavement modulus back-calculation employs a simplified stress–strain relationship (Hooke's Law), assuming that the material is linearly elastic and isotropic and the pavement deformation is small:

$$\sigma_z = \lambda\varepsilon_x + \lambda\varepsilon_y + (\lambda + 2G)\varepsilon_z \tag{5}$$

$$G = \frac{E}{2(1+\mu)} \tag{6}$$

$$\lambda = \frac{2\mu G}{1-2\mu} \tag{7}$$

where σ_z = vertical stress; ε_x, ε_y, ε_z = transverse, longitudinal, and vertical strains, respectively; μ = Poisson's ratio of the material; λ = Lamé's first parameter; and G = shear modulus.

In substituting Equations (6) and (7) into Equation (5) and simplifying, the following is obtained:

$$E = \frac{(1-2\mu)(1+\mu)\sigma_z}{\mu\varepsilon_x + \mu\varepsilon_Y + (1-\mu)\varepsilon_z} \tag{8}$$

According to the requirements of specification, Poisson's ratio of the pavement asphalt mixture is defined as μ = 0.25. In substituting this value into Equation (8) and simplifying, the back-calculation formula for the elastic modulus can be derived as

$$E = \frac{2.5\sigma_z}{\varepsilon_x + \varepsilon_Y + 3\varepsilon_z} \tag{9}$$

In comparing the back-calculated elastic modulus results across sections treated with different grouting materials, the effectiveness of grouting rehabilitation can be quantitatively evaluated.

3. Materials and Methods

3.1. Case Study

Based on the distress characteristics of asphalt pavement along the SCE, this study selected seven sections with semi-rigid base cracking for a comparative analysis of grouting treatment efficacy. Given that all seven selected cross-sections were located within the same road segment, they share identical pavement structures and service durations. Each section exhibits reflective cracks induced by the shrinkage cracking of the semi-rigid base layer, thereby excluding pavement failure caused by subgrade settlement or drainage deficiencies. Among these, the first five sections received distinct grouting materials (detailed in Table 1), where Section 6 served as an untreated control group, and Section 7 represented intact pavement without cracks.

Table 1. Grouting materials and methods for different sections.

Section	Material and Method
Section 1	High-Strength Geopolymer (with waterproofing agent)
Section 2	High-Strength Geopolymer (without waterproofing agent)
Section 3	Low-Strength Geopolymer (without waterproofing agent)
Section 4	Low-Strength Geopolymer (with waterproofing agent)
Section 5	High-Polymer Content
Section 6	Untreated
Section 7	Intact

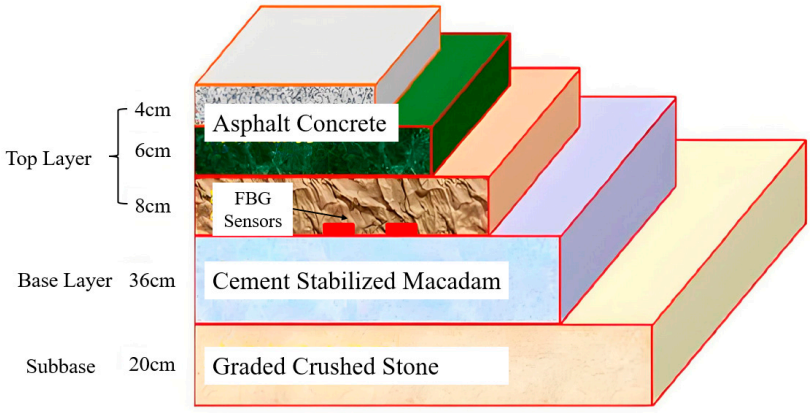
3.2. Sensors Deployment

3.2.1. Deployment Scheme

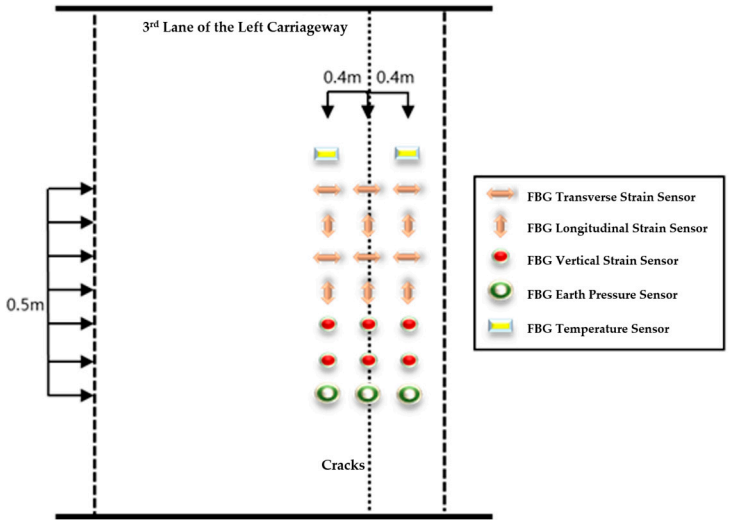
As outlined in Equation (9), modulus back-calculation requires the precise acquisition of four mechanical responses under vehicular loading. To achieve this, each section was instrumented with a tri-columnar FBG sensor array comprising 6 transverse strain sensors, 6 longitudinal strain sensors, 6 vertical strain sensors, 3 Earth pressure sensors, and 2 temperature sensors.

The purpose of setting up the temperature sensor was to monitor the changes in the elastic modulus of the asphalt pavement at different temperatures over a long period of time. However, since the data collection of the loading in this test was carried out almost all within the same period of time (approximately 9 p.m.), the variation in pavement temperature was very small, and thus, the contribution of the temperature sensor was not significant.

The central longitudinal sensor column was positioned directly over pavement cracks, while lateral columns monitored adjacent intact areas, establishing a comparative framework for evaluating localized modulus enhancements post-grouting. This triaxial monitoring configuration enables differential analysis of mechanical responses across treated zones, untreated regions, and reference sections. Figure 3 illustrates the sensor deployment schematic for representative sections.



(**a**)



(**b**)

Figure 3. Schematic of sensors deployment plan. (**a**) Pavement structure layer and placement of sensors; (**b**) sensor layout plan.

3.2.2. On-Site Installation Process

Successful sensor installation for extended monitoring must fulfill four critical criteria:

- Operational viability of sensors.
- Effective strain transfer mechanisms.
- Accessible transmission line routing.
- Seamless system integration.

As depicted in Figure 4, the sensor deployment process was specifically adapted to the experimental road conditions. To ensure measurement accuracy, survival rate, and long-term durability, field implementation followed the following key steps:

(1) Pavement Preparation

Firstly, a 5 m × 2 m rectangular area was milled at sensor installation locations to expose the base layer. Then, an adjacent transverse milling zone spanning at least 0.4 m in width was created perpendicular to the traffic direction within the fourth lane, specifically designed to enable organized cable convergence and routing. Notably, a deliberate buffer distance was maintained between the sensor installation zones and nearby construction joints, thereby ensuring structural discontinuities remained isolated from critical measurement areas.

(2) Sensor Positioning and Installation

The installation process commenced with the precise marking of pre-embedded sensor locations using measuring tapes and spray paint, followed by trench excavation and the removal of oversized aggregates. Subsequently, total stations and straightedges were employed to achieve millimeter-level positioning accuracy, after which cold asphalt patching material was applied to level the trench base, manually compacted with iron hammers. Upon sensor placement, miniature spirit levels and bullseye levels were utilized to align earth pressure sensors and vertical strain sensors, respectively, ensuring pure vertical force transmission without parasitic horizontal components during loading.

(3) Cables Management

Sensor cables were systematically organized and securely bundled to prevent accidental tension-induced damage, while exit points were reinforced with corrugated protective sleeves to mitigate mechanical abrasion risks.

(4) Backfilling and Compaction

Following sensor installation, trenches were backfilled with cold asphalt patching material and subjected to initial manual compaction. Upper structural layers were subsequently paved and rolled across the full pavement section, with vibratory compaction strictly prohibited near sensor arrays to prevent damage or positional displacement.

(5) Documentation and Protection

Finally, the precise locations and identification numbers of the sensors were recorded. The cables were protected and routed into junction boxes, with warning signs installed nearby. Simultaneously, waterproof and anti-corrosion treatments were applied to the sensor cables, and excess cables were properly managed for future connection to the main fiber optic trunk.

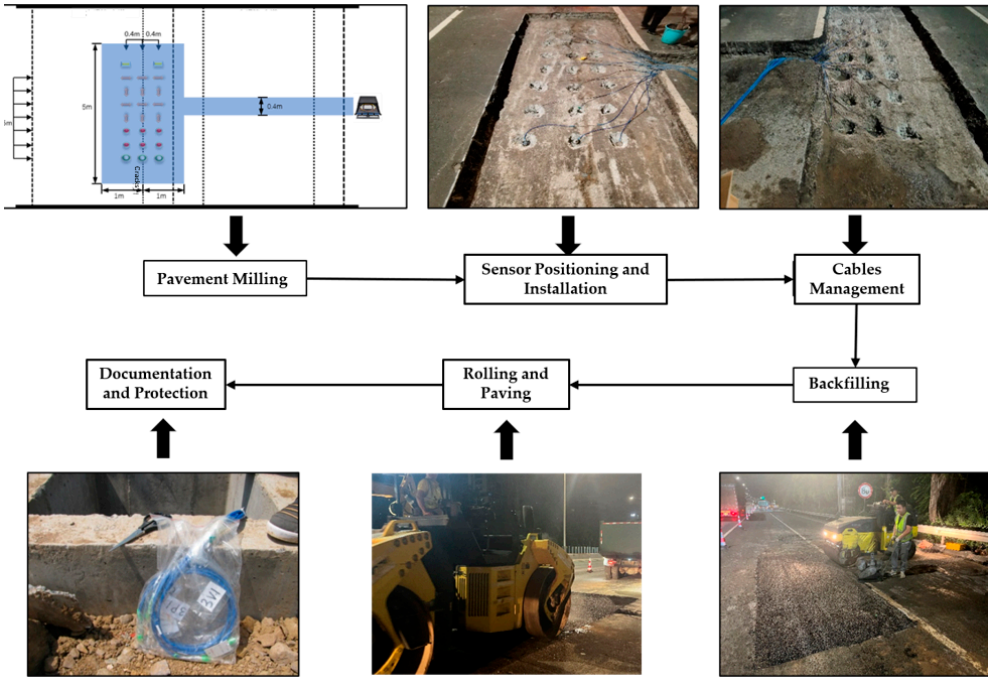


Figure 4. Process of FBG sensor installation.

3.3. Data Acquisition and Processing Protocol

The FBG sensor cables were routed through grooves and connected to the demodulation device. Under operational traffic conditions, the sensor arrays embedded within the pavement structure recorded mechanical responses of the asphalt layer whenever vehicles traversed the seven monitored cross-sections, as illustrated in Figure 5. Given the high vehicle speeds on the SCE, the FBG interrogator was configured with a 1 kHz sampling frequency to ensure real-time data accuracy, utilizing a built-in network interface card for seamless data transmission and export.

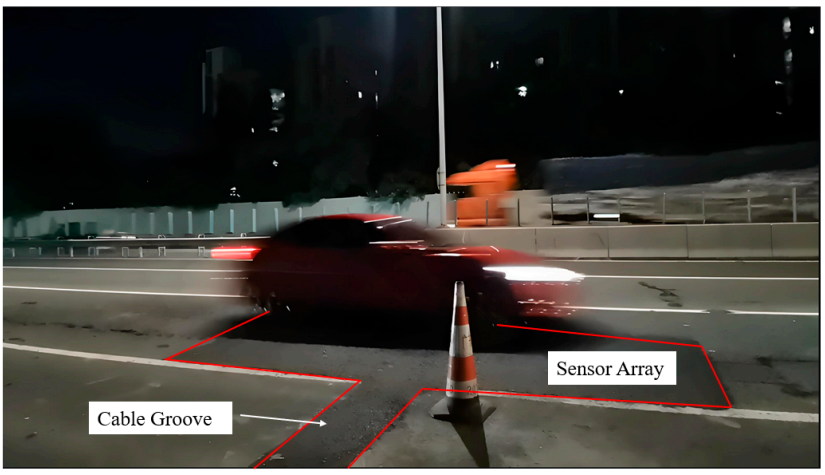


Figure 5. Loading scenarios of actual vehicle passages.

The experimental road section experienced high traffic volume, and the monitoring system operated at a high sampling frequency, necessitating the preprocessing of the collected massive datasets to extract valid signals. Due to the inherent randomness in vehicle axle configurations, load magnitudes, and travel paths, significant variations in wavelength shifts were observed by the sensors. Consequently, this study focused on the statistical patterns of modulus outcomes. By analyzing the mechanical response data

from numerous vehicle passes, the mean elastic modulus and standard deviation were calculated for each section, enabling a scientifically quantitative evaluation of the grouting effectiveness across different materials.

4. Results

4.1. Measured Values of Pavement Mechanical Response

When a vehicle enters the monitored cross-section, the wavelengths of the strain and stress FBG sensors exhibit measurable shifts. As the vehicle traverses the section, pavement deformation recovers, and the sensor wavelengths return to their baseline values, as illustrated in Figure 6. The stress–strain response induced by vehicular loading is derived from these wavelength shifts. Due to variations in vehicle types, heavier axles generate larger strain and stress magnitudes, evidenced by distinct peak variations in Figure 6. To isolate the impact of individual axles during modulus back-calculation, only the maxi-mum peak wavelength shift corresponding to strain and stress from a single vehicle pas-sage was selected for analysis.

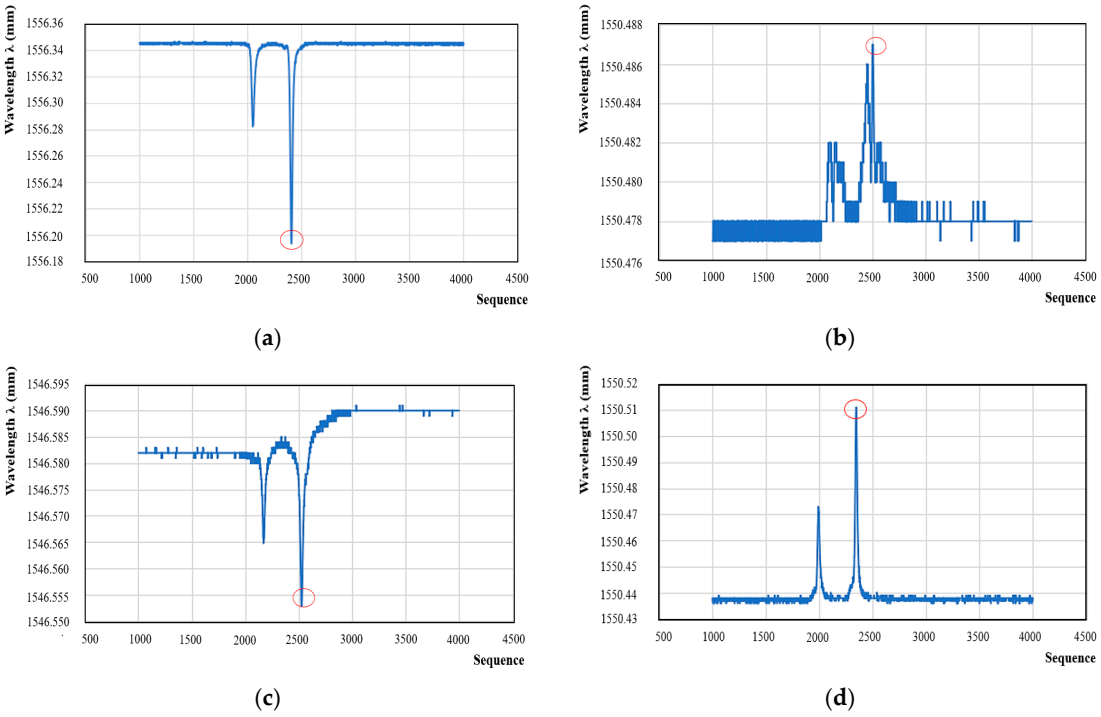


Figure 6. The wavelength change of the sensors when a two-axle vehicle passed by. The red circles represent the peak response value used for subsequent calculations. (**a**) Vertical strain sensor; (**b**) longitudinal strain sensor; (**c**) transverse strain sensor; (**d**) vertical stress sensor.

Due to space constraints, Table 2 presents only the mechanical response data measured by the central column sensors in each cross-section during the passage of a randomly selected vehicle. Preliminary observations indicate that pavements treated with high-strength geopolymer and polymer grouts exhibit superior mechanical performance. Low-strength geopolymer without waterproofing agents exhibits significantly increased vertical strain under humid conditions, leading to susceptibility to cracking and deformation. The addition of waterproofing agents improves vertical strain by mitigating water erosion, though transverse strain remains higher than in high-strength systems. Untreated conventional materials are most affected by loading and water erosion, showing pronounced vertical and transverse strains. Additionally, crack-free construction sections validate the practical effectiveness of theoretical material performance, demonstrating stable stress–strain

behavior and well-controlled transverse deformation. Crucially, the back-calculation of pavement elastic modulus incorporated the statistical analysis of mechanical response data from a large sample of randomly selected vehicles, ensuring enhanced representativeness of the results.

Table 2. Mechanical response of different sections when a random vehicle passed by.

Section	Vertical Stress (MPa)	Vertical Strain (με)	Longitudinal Strain (με)	Transverse Strain (με)
Section 1	0.034	−115	−2	−14
Section 2	0.071	−125	−4	−24
Section 3	0.117	−327	−6	−36
Section 4	0.066	−118	−3	−50
Section 5	0.046	−83	−3	−21
Section 6	0.081	−149	−7	−27
Section 7	0.022	−90	−1	−10

4.2. Back-Calculated Results of Elastic Modulus

The mechanical response data of the pavement under vehicular loads, as monitored by the sensors, were calculated using Equation (9) to determine the average elastic modulus and standard deviation of the asphalt pavement across seven sections. These results were visualized through bar charts for intuitive analysis.

4.2.1. High-Strength Geopolymer

The back-calculated elastic modulus results for Section 1 after grouting treatment are shown in Figure 7a. For the untreated original pavement, the average elastic modulus of asphalt on the left side was 516.38 MPa with a standard deviation of 28.94 MPa. Following treatment with high-strength geopolymer with waterproofing agents, the average elastic modulus increased to 614.69 MPa. And the standard deviation decreased to 22.77 MPa. This represents a 19% improvement in elastic modulus, indicating enhanced material stiffness, while the reduced standard deviation suggests improved uniformity and consistency in performance.

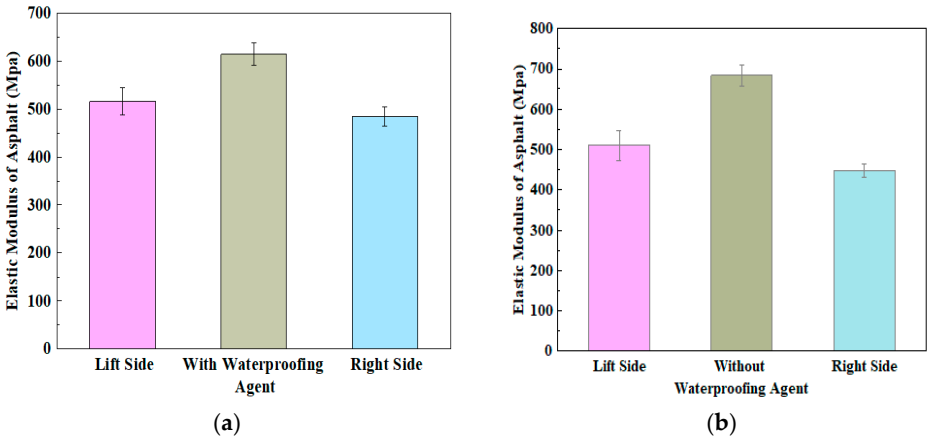


Figure 7. Elastic modulus of asphalt with high-strength geopolymer grouting. (**a**) Section 1; (**b**) Section 2.

Figure 7b presents the results for Section 2. Following the application of high-strength geopolymer without waterproofing agents, the pavement's average elastic modulus of asphalt increased from 509.37 MPa to 682.98 MPa, with the standard deviation decreasing from 37.36 MPa to 25.30 MPa. The elastic modulus significantly increased by approximately

34%, indicating enhanced overall material stiffness. Concurrently, the reduced standard deviation demonstrates improved consistency in elastic modulus measurements, reflecting greater performance stability.

The comparison of Sections 1 and 2 shows that the high-strength geopolymer without waterproofing agents exhibited better short-term mechanical performance, achieving a higher average elastic modulus. The smaller modulus difference between the left and right lanes indicates more uniform structural stress distribution, particularly in load transfer equilibrium between lane edges and centers. This suggests that the non-waterproofed formulation provides superior interfacial bonding and stress redistribution in practical engineering applications. This phenomenon may be attributed to the interference of waterproofing agents in the alkali activation reaction of geopolymers, leading to incomplete polymerization during the early stages. Materials without waterproofing agents undergo more thorough reactions, forming a denser three-dimensional microstructure in the short term, thereby achieving a higher elastic modulus.

4.2.2. Low-Strength Geopolymer

The back-calculated elastic modulus results for Section 3 after grouting treatment are shown in Figure 8a. The average elastic modulus of asphalt in the pavement treated with low-strength geopolymer (without waterproofing agents) was 517.10 MPa, comparable to the left-side pavement and slightly higher than the right-side pavement, with a standard deviation of 15.44 MPa. The data indicate concentrated elastic modulus values for this material, with the lower standard deviation suggesting more consistent performance and reduced variability.

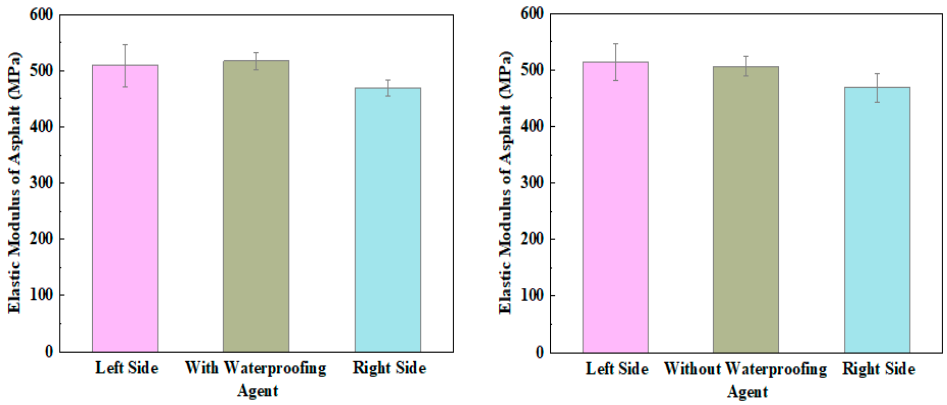


Figure 8. Elastic modulus of asphalt with low-strength geopolymer grouting. (**a**) Section 3; (**b**) Section 4.

The back-calculated asphalt elastic modulus results for Section 4 after grouting treatment are shown in Figure 8b. The pavement treated with low-strength geopolymer (with waterproofing agents) exhibited an average elastic modulus of 505.37 MPa, slightly lower than that of the left-side pavement, with a standard deviation of 17.16 MPa. These results indicate relatively uniform material performance (lower variability) but reduced strength, suggesting poor grouting effectiveness for this formulation.

Compared to the back-calculated asphalt elastic modulus results of high-strength geopolymer-treated pavements (Sections 1 and 2), the low-strength geopolymer treatment yielded a significantly lower average elastic modulus, indicating lower material strength. This performance suggests its suitability for secondary roads or light-load structures.

4.2.3. High-Polymer Materials

High-polymer materials typically exhibit superior strength performance, making them suitable for high-load applications. The back-calculated elastic modulus results for Section 5 after high-polymer grouting treatment are shown in Figure 9. As illustrated, the grouting-treated pavement achieved an average elastic modulus of 676.15 MPa, significantly higher than that of the untreated adjacent areas, indicating exceptional stiffness and excellent mechanical properties. The relatively low standard deviation of 25.04 MPa further demonstrates consistent performance across test points, confirming uniform material behavior.

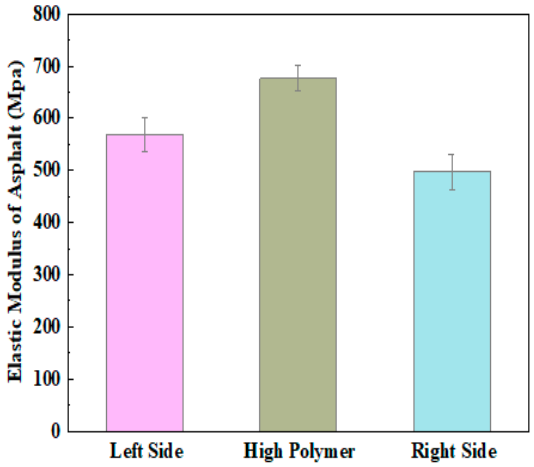


Figure 9. Elastic modulus of asphalt with high-polymer grouting.

4.2.4. Untreated and Intact Sections

The back-calculated elastic modulus results for Sections 6 and 7 are shown in Figures 10 and 11, respectively. For the cracked pavement (Section 6), the average elastic modulus of asphalt was 415.40 MPa, significantly lower than for both the left-side and right-side pavements, demonstrating that cracks substantially reduce structural strength and load-bearing capacity. In contrast, the crack-free pavement (Section 7) exhibited an average elastic modulus of 479.74 MPa, lower than for the left-side pavement but higher than for the right-side pavement, indicating relatively favorable material stiffness and moderate load-bearing capability in this intact region.

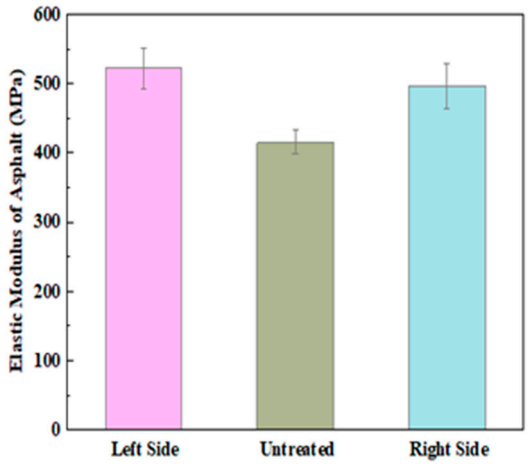


Figure 10. Elastic modulus of asphalt in untreated cracked section.

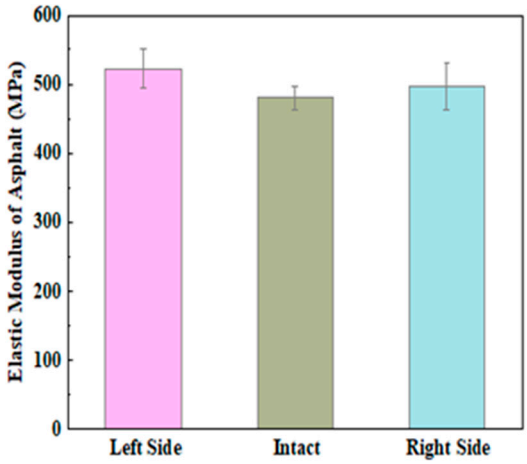


Figure 11. Elastic modulus of asphalt in crack-free intact section.

4.2.5. Comparison and Discussion

A comparative analysis of the seven cross-sections, as shown in Figure 12, reveals the following ranking of average asphalt elastic modulus values for the asphalt pavement treated with different materials: high-strength geopolymer (without waterproofing agents) > polymer > high-strength geopolymer (with waterproofing agents) > low-strength geopolymer (without waterproofing agents) > low-strength geopolymer (with waterproofing agents) > intact pavement > untreated pavement. The results demonstrate that high-strength geopolymer (without waterproofing agents) and high-polymer materials exhibit optimal performance, with their post-grouting average elastic moduli significantly exceeding those of other sections. These materials are well-suited for grouting-based crack rehabilitation in this roadway, offering superior mechanical properties and structural reinforcement under operational traffic loads.

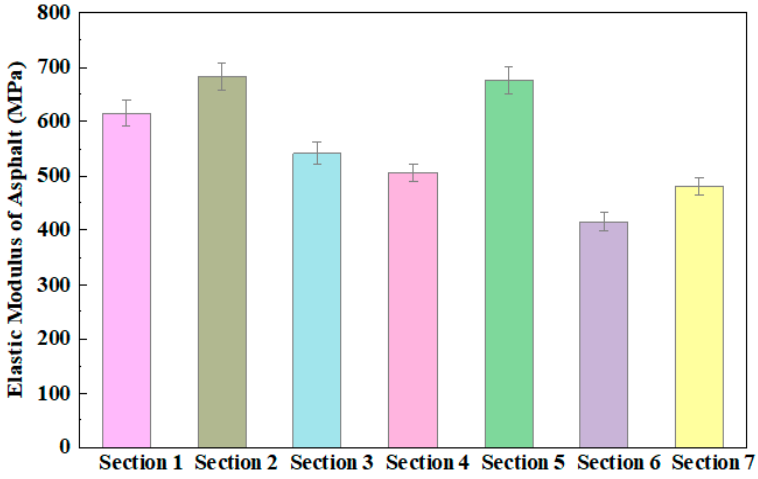


Figure 12. Comparison of elastic modulus for seven sections.

High-strength geopolymer and high-polymer materials are widely regarded as effective solutions for enhancing pavement performance due to their exceptional mechanical properties, a perspective further substantiated by the quantitative data provided in this study. While the current research offers valuable short-term performance insights, comprehensive long-term performance evaluations under operational conditions remain critical for future investigations. Therefore, subsequent studies should prioritize the following:

(1) Long-term durability assessment of grouting materials under diverse environmental conditions.

(2) Sensor deployment optimization to quantify the influence of sensor configurations on data integrity and strain measurement accuracy.
(3) Algorithmic refinement of modulus back-calculation methodologies by integrating multi-axial stress coupling models.

These advancements will enhance the accuracy and applicability of research findings, enabling predictive maintenance frameworks for sustainable pavement management.

5. Conclusions

This study investigated the mechanical responses of asphalt pavements under traffic loads using fiber Bragg grating (FBG) sensing technology and evaluated the performance of various grouting materials, yielding the following conclusions:

(1) By deploying FBG sensors at the top of the pavement base layer, this study collected real-time mechanical response data under extensive vehicular loading. Through comparative analysis of mechanical response characteristics across sections and using the back-calculated pavement elastic modulus as an evaluation metric, an assessment methodology for grouting treatment effectiveness on cracks in semi-rigid base asphalt pavements was proposed. The findings provide guidance for the design of grouting materials, optimization of injection processes, and post-treatment maintenance strategies for semi-rigid base asphalt pavements.
(2) High-strength geopolymer grouting materials significantly improved pavement mechanical performance. The average elastic modulus of asphalt increased by 34% for high-strength geopolymer without waterproofing agents and 19% for the variant with waterproofing agents. Polymer grouting achieved an average elastic modulus of 676.15 MPa, demonstrating notable enhancement. In contrast, low-strength geopolymers showed limited efficacy, with minimal changes in pavement modulus. These findings confirm the superior performance of high-strength geopolymers and polymers, making them suitable for high-load road structures. The ranking of average elastic modulus values across treated sections is as follows: high-strength geopolymer (without waterproofing agents) > polymer > high-strength geopolymer (with waterproofing agents) > low-strength geopolymer (without waterproofing agents) > low-strength geopolymer (with waterproofing agents) > intact pavement > untreated pavement.

This study evaluated the short-term effectiveness of grouting treatments. Subsequent research should investigate the long-term performance of grouting materials under diverse environmental conditions (e.g., varying temperatures, moisture levels). The accuracy of this methodology can be further validated by integrating FWD field data and numerical simulation results. Furthermore, more refined sensor deployment configurations and optimized modulus back-calculation algorithms should be implemented to enhance the accuracy and applicability of research outcomes.

Author Contributions: Conceptualization, M.Z. and H.H.; data curation, Z.S.; formal analysis, X.M.; funding acquisition, M.Z. and H.H.; investigation, M.Z.; methodology, X.M.; project administration, M.Z. and H.H.; resources, H.H.; supervision, X.M.; validation, C.R., Z.S. and X.M.; visualization, Z.S.; writing—original draft, C.R.; writing—review and editing, C.R. and X.M. All authors have read and agreed to the published version of the manuscript.

Funding: This research was funded by the National Natural Science Foundation of China (Grant No. 52478451) and technology project of Guangzhou Suihua Intelligent Traffic Technology Co., Ltd.

Institutional Review Board Statement: Not applicable.

Informed Consent Statement: Not applicable.

Data Availability Statement: The original contributions presented in this study are included in the article. Further inquiries can be directed to the corresponding author.

Conflicts of Interest: The authors declare that this study received funding from Guangzhou Suihua Intelligent Traffic Technology Co., Ltd. The funder was not involved in the study design, collection, analysis, interpretation of data, the writing of this article or the decision to submit it for publication. And authors Min Zhang and Hongbin Hu were employed by the company Guangzhou Suihua Intellignet Traffic Technology Co., Ltd. The remaining authors declare that the research was conducted in the absence of any commercial or financial relationships that could be construed as a potential conflict of interest.

Abbreviations

The following abbreviations are used in this manuscript:

FBG	Fiber Bragg grating;
SCE	The South China Expressway;
FWDs	Falling weight deflectometers.

References

1. Shi, Z.; Yue, J.; Xu, L.; Wang, X. Peridynamics for Fracture Analysis of Reflective Cracks in Semi-Rigid Base Asphalt Pavement. *Appl. Sci.* **2022**, *12*, 3486. [CrossRef]
2. Yao, L.; Leng, Z.; Jiang, J.; Fang, C.; Ni, F. Effects of Traffic Load Amplitude Sequence on the Cracking Performance of Asphalt Pavement with a Semi-Rigid Base. *Int. J. Pavement Eng.* **2023**, *24*, 2152027. [CrossRef]
3. Wang, X.; Zhong, Y. Reflective Crack in Semi-Rigid Base Asphalt Pavement Under Temperature-Traffic Coupled Dynamics Using XFEM. *Constr. Build. Mater.* **2019**, *214*, 280–289. [CrossRef]
4. Chen, Z.; Qiao, J.; Yang, X.; Sun, Y.; Sun, D. A Review of Grouting Materials for Pouring Semi-Flexible Pavement: Materials, Design and Performance. *Constr. Build. Mater.* **2023**, *379*, 131235. [CrossRef]
5. Fang, H.; Zheng, Q.; Du, M.; Liu, J.; Zhang, C.; Wang, Z.; Wang, F. Study of the Mechanical Properties and Constitutive Model of the Roadbed Rehabilitation Polyurethane Grouting Materials under Uniaxial Compression. *J. Appl. Polym. Sci.* **2022**, *139*, 52276. [CrossRef]
6. Wang, Z.; Du, M.; Fang, H.; Zhang, C.; Li, M.; Shi, M. Influence of Different Corrosion Environments on Mechanical Properties of a Roadbed Rehabilitation Polyurethane Grouting Material under Uniaxial Compression. *Constr. Build. Mater.* **2021**, *301*, 124092. [CrossRef]
7. Zhang, C.; Yang, J.; Fu, J.; Wang, S.; Yin, J.; Ou, X.F.; Xie, Y. Optimal Formulation Design of Polymer-Modified Cement Based Grouting Material for Loose Deposits. *Constr. Build. Mater.* **2020**, *261*, 120513. [CrossRef]
8. Peng, H.; Zhang, B. Research Progress on the Durability of Geopolymer Concrete. *J. Changsha Univ. Sci. Technol. Nat. Sci.* **2023**, *20*, 1–24. [CrossRef]
9. Sarıdemir, M.; Çelikten, S. Effect of High Temperature, Acid and Sulfate on Properties of Alkali-Activated Lightweight Aggregate Concretes. *Constr. Build. Mater.* **2022**, *317*, 125886. [CrossRef]
10. Hamid Abed, M.; Sabbar Abbas, I.; Hamed, M.; Canakci, H. Rheological, Fresh, and Mechanical Properties of Mechanochemically Activated Geopolymer Grout: A Comparative Study with Conventionally Activated Geopolymer Grout. *Constr. Build. Mater.* **2022**, *322*, 126338. [CrossRef]
11. Li, S.; Niu, Y.; Wang, B.; Gao, Y.; Zhu, Y. Research on Mechanical Response of Polymer Grouting Repair for Longitudinal Cracks in Reconstructed and Expanded Expressway Pavement. *Math. Probl. Eng.* **2022**, *2022*, 5760674. [CrossRef]
12. Zhu, H.; Xu, H.; Wei, G.; Yu, X.; Ma, D.; Tang, Y.; Ma, H. Evaluation of Grouting Effectiveness for Semi-Rigid Pavement Base Layer Cracks Based on Time-Frequency Domain Signal Characteristics of 3D GPR. *Measurement* **2024**, *237*, 115228. [CrossRef]
13. Zhang, B.; Zhang, X.; Zhong, Y.; Li, X.; Hao, M.; Sang, X.; Wang, X.; Liu, J. Research on Fatigue Model of Semi-Rigid Base Asphalt Pavement before and after Polymer Grouting. *Adv. Civ. Eng.* **2021**, *2021*, 6658943. [CrossRef]
14. Li, Z.; Liu, J.; Xu, R.; Liu, H.; Shi, W. Study of Grouting Effectiveness Based on Shear Strength Evaluation with Experimental and Numerical Approaches. *Acta Geotech.* **2021**, *16*, 3991–4005. [CrossRef]
15. Ramakrishnan, M.; Rajan, G.; Semenova, Y.; Farrell, G. Overview of Fiber Optic Sensor Technologies for Strain/Temperature Sensing Applications in Composite Materials. *Sensors* **2016**, *16*, 99. [CrossRef]
16. Geng, L.T.; Ren, R.B.; Zhong, Y.; Xu, Q. Application of FBG Sensors in Flexible Pavement Monitoring. *Adv. Mater. Res.* **2011**, *255–260*, 3397–3403. [CrossRef]

17. Wang, H.-P.; Wu, Y.-B.; Zhang, C.; Xiang, P. Monitoring Data Motivated Health Condition Assessment of Cement Concrete Pavements in Field Based on FBG Sensing Technology. *Struct. Health Monit.* **2024**, 14759217241268821. [CrossRef]
18. Chen, Y.; Wu, J.; Lin, D.; Zhao, X.; Zhang, L. Research on Dynamic Response of Vertical Displacement of Runway Pavement Slab End Under Aircraft Taxiing Using Novel FBG Sensors. *Measurement* **2025**, *243*, 116296. [CrossRef]
19. Kara De Maeijer, P.; Van Den Bergh, W.; Vuye, C. Fiber Bragg Grating Sensors in Three Asphalt Pavement Layers. *Infrastructures* **2018**, *3*, 16. [CrossRef]
20. Huang, H.; Yuan, S. Study on the Spectral Response of Fiber Bragg Grating Sensor Under Non-Uniform Strain Distribution in Structural Health Monitoring. *Optoelectron. Lett.* **2011**, *7*, 109–112. [CrossRef]
21. Kersey, A.D.; Davis, M.A.; Patrick, H.J.; LeBlanc, M.; Koo, K.P.; Askins, C.G.; Putnam, M.A.; Friebele, E.J. Fiber Grating Sensors. *J. Light. Technol.* **1997**, *15*, 1442–1463. [CrossRef]

Disclaimer/Publisher's Note: The statements, opinions and data contained in all publications are solely those of the individual author(s) and contributor(s) and not of MDPI and/or the editor(s). MDPI and/or the editor(s) disclaim responsibility for any injury to people or property resulting from any ideas, methods, instructions or products referred to in the content.